



A EUROPEAN JOURNAL

# CHEMPHYSCHEM

OF CHEMICAL PHYSICS AND PHYSICAL CHEMISTRY

## Accepted Article

**Title:** Synchrotron Photoionization Study of the Diisopropyl Ether Oxidation

**Authors:** Andrea Giustini and Giovanni Meloni

This manuscript has been accepted after peer review and appears as an Accepted Article online prior to editing, proofing, and formal publication of the final Version of Record (VoR). This work is currently citable by using the Digital Object Identifier (DOI) given below. The VoR will be published online in Early View as soon as possible and may be different to this Accepted Article as a result of editing. Readers should obtain the VoR from the journal website shown below when it is published to ensure accuracy of information. The authors are responsible for the content of this Accepted Article.

**To be cited as:** *ChemPhysChem* 10.1002/cphc.201901134

**Link to VoR:** <http://dx.doi.org/10.1002/cphc.201901134>

WILEY-VCH

[www.chemphyschem.org](http://www.chemphyschem.org)

A Journal of



# Synchrotron Photoionization Study of the Diisopropyl Ether Oxidation

Andrea Giustini \*      Giovanni Meloni\*<sup>†‡</sup>

February 11, 2020

## 1 Abstract

Scientific evidence has shown oxygenates help to reduce dangerous pollutants arising from burning fossil fuel in the automotive sector. For this reason, their use as additives has spread widely. The aim of this work consists in providing a comprehensive identification of the main primary oxidation products of diisopropyl ether (DIPE), one of the most promising among etheric oxygenates. The Cl-initiated oxidation of DIPE is examined by using a vacuum ultraviolet (VUV) synchrotron radiation at the Advanced Light Source (ALS) of the Lawrence Berkeley National Laboratory (LBNL). Products are identified on the basis of their mass-to-charge ratio, shape of photoionization spectra, adiabatic ionization energies, and chemical kinetic profiles, at three different temperatures (298, 550, and 650 K). Acetone, propanal, propene, and isopropyl acetate have been identified as major reaction products. Acetone is the main primary product. Theoretical calculations using the composite CBS-QB3 method provided useful tools to validate the postulated reaction mechanisms leading to experimentally observed species. The formation of other species is also discussed.

\*A. Giustini and Prof. G. Meloni, Department of Physical and Chemical Sciences, University of L'Aquila, L'Aquila (Italy)

<sup>†</sup>Prof. G. Meloni, Department of Chemistry, University of San Francisco, San Francisco, California 94117 (United States)

<sup>‡</sup>corresponding author

## 2 Introduction

Air pollution arising from automotive emissions is to date a point of major concern in terms of health hazards and environmental consequences. Indeed, other than carbon dioxide (CO<sub>2</sub>) and water vapor (H<sub>2</sub>O), the combustion process can lead to the formation of many species, including carbon monoxide (CO), uncombusted hydrocarbons (HCx), nitrogen oxides (NOx), and volatile organic compounds (VOCs). CO and HCx are obtained when internal combustion engines run during a rich regime, hence a lower amount of oxygen is available leading to incomplete combustion. NOx formation is very rapid at high temperature, especially when air-fuel equivalence ratio goes rich.[1] VOCs are a mixture of hydrocarbons and aromatic compounds, with the latter being carcinogenic and mutagenic according to scientific evidences, thus with serious health effects on human life.[2, 3] They also have been shown to be able to enhance the tropospheric ozone levels during summertime when the sunlight is the highest and the probability of photochemical-ozone-precursor production is higher.[4] Great effort has been made to reduce pollutants deriving from fossil fuel consumption. The elimination of lead and aromatic molecules as anti-knock compounds (octane-enhancer) from gasoline has been the first step to meet this goal, but it drove the need to find valid alternative options to replace the lost octane number.[1]

Oxygenates matched these requirements and over the last three decades they have started to be added to gasoline in order to get blends providing for cleaner-burning fuel.[5] The presence of oxy-

gen, indeed, guarantees a complete combustion resulting into lower CO, HCx, and toxic exhausts, but slightly higher NOx release, besides improving engine performance.[6] No particular benefits have been recorded in terms of reducing greenhouse gas emissions. The replacement of aromatic components with oxygenates causes the fuel-burning process to be more energy-efficient, resulting into CO<sub>2</sub> increase.[5] Among oxygenates, diisopropyl ether (hereafter: DIPE) has been recognized as one of the best fuel additives due to its excellent capability to blend with gasoline.[7] DIPE also exhibits a much lower water solubility and volatility, as well as a lack of toxicity with respect to methyl tert-butyl ether (MTBE), the most used oxygen-containing additive in the United States until 2000.[8–11] Such properties are essential to prevent the dispersion in the environment, which could cause groundwater contamination with dangerous effect on both human health and ecosystem in general. In order to fully assess DIPE environmental impact, an in-depth evaluation of its combustion features is needed before endorsing its effective usage as alternative oxygenate.[12] DIPE is initially obtained by hydration of propylene into isopropanol, followed by addition of another propylene molecule to yield the desirable ether. A parallel competitive dehydrative reaction of isopropanol can lead to the formation of DIPE. Both the etherification and hydration reactions are exothermic and reversible.[7, 13] In recent years, researchers investigated the oxidation of DIPE by focusing on several reaction pathways. Collins and co-workers[14] studied the OH radical-initiated oxidation in the presence and absence of NOx. They found various products, such as isopropyl acetate, formaldehyde, and acetone, which are formed through reactions based on C-C and C-O bond fission, and isomerisation mechanisms. In Wang et al. work[15], quantum chemistry calculations are carried out to evaluate atmospheric oxidation of three different ethers, including DIPE. They focused onto hydrogen abstraction by OH radicals with and without NOx. Similarities with Collins' work[14] have been reported, confirming isopropyl acetate as the major product in the presence of NOx and acetone when NOx are missing. Discrepancies have been reported just for the proposed reaction

mechanisms leading to them.

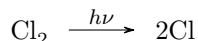
This study aims to provide information about the oxidation of DIPE relevant for determining its environmental impact. Characterization of primary products was performed by investigating the Cl-initiated oxidation process at three different temperatures. In addition, electronic structure calculations were carried out to explore the feasible reaction pathways leading to products formation, giving key insights on the explanation of experimental data sets.

### 3 Experimental Section

Experiments were performed at the Chemical Dynamics beamline of the Advanced Light Source (ALS) situated at the Lawrence Berkeley National Laboratory (California, USA). A tunable synchrotron radiation (7.2 - 25 eV) is used coupled with a multiplexed (all species detected simultaneously) time- and energy-resolved mass spectrometer to probe reaction species. Further details about the experimental apparatus are discussed in previous works.[16–19]

The vapors of DIPE (Sigma-Aldrich, 99.0%) are collected in a gas cylinder to reach an overall concentration of about 1.0% in excess of helium. In this work, DIPE reacts with O<sub>2</sub> in the presence of the radical precursor Cl<sub>2</sub> at room temperature, 550, and 650 K and a pressure of 4, 7, and 7 Torr, respectively. Gaseous reactants are directed into a 62 cm long slow-flow quartz reaction tube and regulated by means of calibrated mass flow controllers. The temperature of the reactor, wrapped by a 18 μm thick nichrome heating tape, can be adjusted according to achieve the desired setup. Additionally, in order to avoid temperature fluctuations, the reactor is surrounded with an insulating square-weave, yttria-stabilized zirconia (ZYW-15, Zircar Zirconia, Inc.) cloth surrounded by two-halves of a gold-plated copper sheath. Further, a feedback controlled throttle valve connects a Roots pump to the reaction tube so that the reactor pressure is allowed to be changed and maintained throughout the experiments. The gas mixture is photolyzed by a 4 Hz-pulsed unfocused 351 nm (XeF) excimer laser, propagating collinearly down the quartz tube. Chlorine atoms are formed according to the

following equation:



The IUPAC Subcommittee for Gas Kinetic Data Evaluation recommended 1.00 as the quantum yield of  $\text{Cl}_2$  photolysis.[20] On the basis of the absorption cross section value at 351 nm that is  $1.82 \times 10^{-19} \text{ cm}^2$  according to Maric et al.[21], the recommended quantum yield, and the concentration of  $\text{Cl}_2$  molecules, which have been calculated to be  $1.29 \times 10^{13}$  molecules  $\text{cm}^{-3}$  at room temperature,  $2.41 \times 10^{13}$  molecules  $\text{cm}^{-3}$  at 550 K, and  $2.04 \times 10^{13}$  molecules  $\text{cm}^{-3}$  at 650 K, the number density for Cl atoms is  $8.33 \times 10^{11}$  to  $1.32 \times 10^{12}$  molecules  $\text{cm}^{-3}$ . Number densities for DIPE are  $2.37 \times 10^{13}$ ,  $2.20 \times 10^{13}$ , and  $2.83 \times 10^{13}$  molecules  $\text{cm}^{-3}$  at 298, 550, and 650 K, respectively; number densities for  $\text{O}_2$  are  $1.29 \times 10^{16}$ ,  $1.20 \times 10^{15}$ , and  $1.03 \times 10^{16}$  molecules  $\text{cm}^{-3}$  at 298, 550, and 650 K, respectively. The reaction species effuse through a  $650 \mu\text{m}$  wide pinhole located on the side of the reactor, then are skimmed into the differentially vacuumed ionization region of the instrument. Once ionized, they are accelerated via a 50 kHz pulsed time-of-flight mass spectrometer with a current mass resolution of 1600 and detected.[22] The photoionization spectrum (PI) of isopropyl acetate (Sigma-Aldrich, 99%) is recorded as well for data analysis. A calibration experiment is performed by flowing known amounts of DIPE and a calibration gas mixture composed by propene, 1-butene, and ethene, without photolysis. Authentic spectra are taken to check the photoionization behaviour of DIPE.

Multiplexed time- and energy-resolved mass spectrometry experiments are developed to scan simultaneously all the species at different photon energies. A tunable synchrotron radiation is used in a quasi-continuous fashion as ions provider starting before the trigger time, which corresponds to the time when the photolysis laser is fired and the radical-generating precursor is decomposed. The photon energy is varied from 9 to 11 eV with a 0.025 eV stepsize. At each photon energy, the ion signal is background (prephotolysis signal) subtracted, and subsequently normalized to the ALS photocurrent, which is measured by a calibrated photodiode located in the ionization re-

gion. In order to extract valuable observables, data sets are sorted out into a 3D data block in which the dimensions are referred to as mass-to-charge ratio, time, and photon energy variables. Data analysis consists of slicing 3D data into 2D images and further into 1D plots to yield photoionization spectra and kinetic traces used for qualitative and quantitative studies. PI curves, for instance, are used to identify species and to distinguish isomers from each other, since their onset, shape, and intensity are strictly correlated to ionization thresholds, Franck-Condon factors, as well as concentration of chemicals. Thus, by comparing literature, measured, or calculated PI curves with experimental data, isomers identification can be achieved. Adiabatic ionization energy (hereafter: AIE) of species is established by linear extrapolation of the initial onset of the photoionization signal as explained elsewhere.[23] Taking into account the photon energy stepsize used for data acquisition and possible existence of hot bands, an overall error of 0.05 eV is estimated for reported AIEs values determined in this work.

## 4 Computational methods

Electronic structure calculations are performed to compute adiabatic ionization energies when unknown. All calculations are carried out by using Gaussian 09 program[24] and the CBS-QB3 composite method.[25, 26] This model has a reported energy mean average deviation of 4-5  $\text{kJ mol}^{-1}$  given by Montgomery et al.[26] AIEs are yielded by the difference between the zero-point corrected total electronic energies (ZPE) of the ground electronic states of the neutral and of the cationic molecules. ZPE are also used to derive enthalpies of reaction ( $\Delta_r H^\circ$ ) useful to demonstrate that a proposed reaction path is thermodynamically feasible.

In addition, the appearance energies (AE) of daughter ions are expressed as follows, if a dissociation barrier is not present:

$$AE = AIE + BDE \quad (1)$$

where BDE is the bond dissociation energy, i.e., the difference between the zero-point energy of the

fragments and the parent ion ground state. AEs are coupled with thermodynamic values to provide useful information regarding enthalpies of formation ( $\Delta_f H^o$ ) of species involved in photodissociative reactions. In fact, since AE is the enthalpy of reaction at 0 K experimentally-derived, and if the other enthalpies of formation are well-known, the third one can be determined as a result of the following equation:

$$\Delta_r H_{0K} = \Delta_f H_{0K}^o(A^+) + \Delta_f H_{0K}^o(B^*) - \Delta_f H_{0K}^o(AB) \quad (2)$$

where AB is the generic neutral molecule,  $A^+$  its cationic fragment, and  $B^*$  its radical fragment. Relaxed potential energy surface (PES) scans were carried out using the B3LYP/6-311G\* level of theory in order to locate possible first order saddle points (transition states) along the PES, and then reoptimized with the CBS-QB3 composite method. The transition states are verified through intrinsic reaction coordinate (IRC) calculations[27] to ensure that the forward and reverse mechanisms fall down into PES minima. If the photoionization spectrum of a reaction species is not found in the literature, it can be measured or, where appropriate, it can be simulated by integrating the photoelectron spectrum generated by approximating the Franck-Condon factors for the vibronic transition from the neutral to the cationic vibrational states of the molecule. These simulations are performed using Franck-Condon (FC)[28–31] and Franck-Condon-Herzberg-Teller methods (FCHT).[28]

## 5 Results and Discussion

Atmospheric oxidation of oxygenates typically begins with a reaction involving OH-radicals, as a result of photolysis reactions due to sunlight. In this work, atomic chlorine is replacing the atmospheric radicals to initiate the hydrogen-abstraction from DIPE. Typically, chlorinated species are obtained from Cl-addition to unsaturated primary products and they are identified on the basis of isotopic ratio for  $^{37}\text{Cl}$  and  $^{35}\text{Cl}$ . However, peaks referring to chlorinated

species are not appearing in the performed experiments. The reaction products are investigated after subtracting the contribution of prephotolysis signals (background).

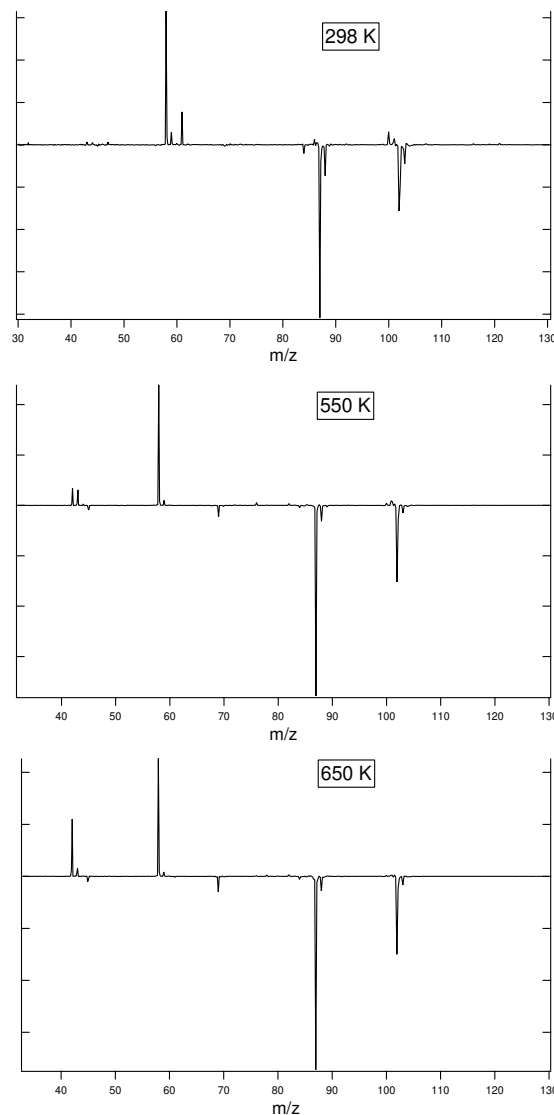


**Figure 1:** Background subtracted mass spectra for Cl-initiated oxidation of DIPE at 298 K, 550 K, 650 K, over the photon energy range of 9.0 to 11.0 eV and over reaction time range 0 - 150 ms.

Mass spectra in Figure 1 reveal negative (reactants signal) and positive (products) peaks. The prominent negative-peak at  $m/z = 87$  corresponds to the main fragment of the photodissociation process of DIPE. The presence of the molecular ion at  $m/z = 102$  also reveals a distinction between DIPE and other ethers, such as MTBE and ETBE, which are characterized by the absence of parent ion signal.[32] Additional daughter ions are recorded at  $m/z = 69$  and  $m/z = 45$ , but they have much lower intensity than  $m/z = 87$  (3 and 0.1 %, respectively). There are not any published experimental photoelectron and authentic photoionization spectra of DIPE for comparison. Williams et al.[33] assigned an ionization energy of 9.16 eV for DIPE, whereas Watanabe et al.[34] gave a value of 9.20 eV, which are in agreement with the experimentally-derived value of  $9.10 \pm 0.05$  eV from this work (see Figure 2).

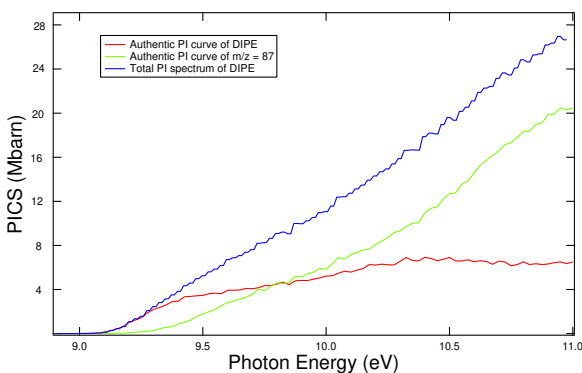


**Figure 2:** Authentic experimental photoionization spectrum of diisopropyl ether.

When photoionization cross-sections of a species are unknown, we used the absolute photoionization spectrum of a reference species to compare with the PI experimental spectrum of the species with a known concentration in order to estimate its  $\sigma_E$ . This estimation comes from the equation defining the ion signal of a species  $i$  at the photon energy  $E$ :

$$S_i(E) = k\sigma_i(E)\delta_i C_i \quad (3)$$

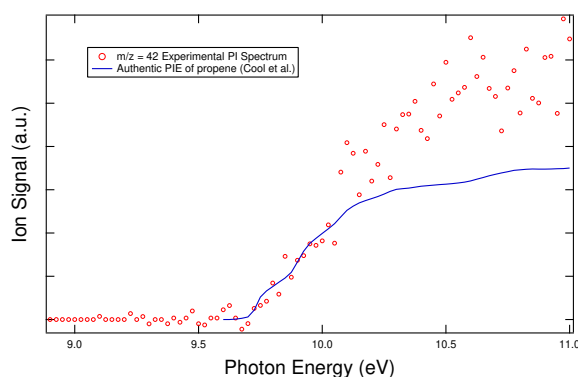
where  $C_i$  is the concentration of the species  $i$ ,  $\sigma_i(E)$  represents the photoionization cross-section of the

species  $i$  at the photon energy  $E$ ,  $k$  is the instrumental constant,  $S_i(E)$  is the ion signal at the specified photon energy, and  $\delta_i$  is the mass discrimination factor that stands for the mass-dependent response of the instrument, here approximately equivalent to the mass of the species  $i$  to the power of 0.67.[35] From the ratio of the signal of the species ( $P$ ) for which we want to determine the photoionization cross-section to the signal of the reference species ( $R$ ), we can derive the desired quantity, as follows:

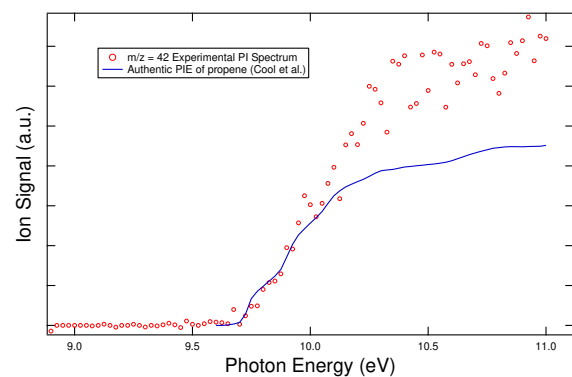
$$\begin{aligned} \sigma_P(E) &= \frac{S_P(E) C_R \delta_R}{S_R(E) C_P \delta_P} \sigma_R(E) \\ &= \frac{S_P(E) C_R}{S_R(E) C_P} \left(\frac{m_R}{m_P}\right)^{0.67} \sigma_R(E) \end{aligned} \quad (4)$$

Figure 2 shows the total absolute photoionization spectrum of diisopropyl ether obtained by summing up DIPE and its most abundant fragment relative cross-sections, estimated by using the above-mentioned method.

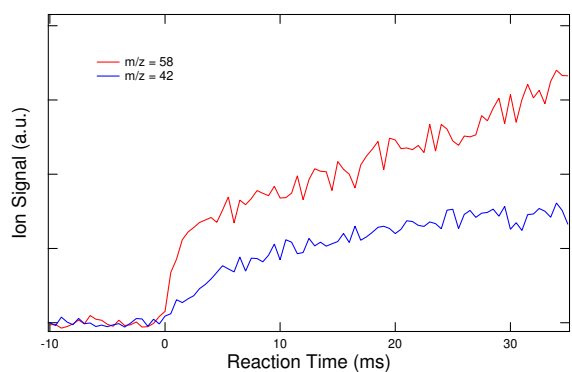
At  $m/z = 42$  a signal grows as the temperature is increased from 550 K up to 650 K (see Figure 3). The experimental onset is measured to be  $9.70 \pm 0.05$  eV, which is in line with the value of  $9.73 \pm 0.02$  eV for propene as observed by Traeger.[36] In order to characterize this mass, propene PI spectrum by Cool[37] has been superimposed onto the experimental plot. The first part is in very good agreement with it, whereas the second part starting from roughly 10.1 eV is not assigned and it may derive from dissociatively photoionizing secondary products. Its time trace is slower than acetone time trace, suggesting it arises from secondary chemistry reactions (see Figure 3c). At  $m/z = 43$ , a signal is detected in the experiments at 550 and 650 K. It was thought to arise from photoionization of isopropyl radicals but the experimental PI spectrum illustrated in Figure 4a shows an onset at around 9.9 eV, which is quite far from literature value of  $7.37 \pm 0.02$  eV[38], suggesting that it is clearly a fragment resulting from a dissociatively photoionizing species. In addition,  $m/z = 43$  kinetic trace in Figure 4b exhibits a fast formation followed by a stable signal, implying the probable involvement of a primary chemistry mechanism.



(a)

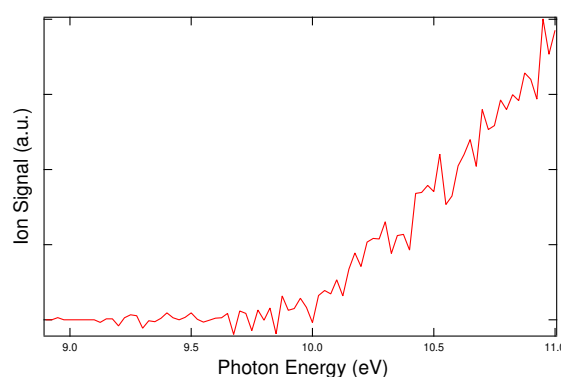


(b)

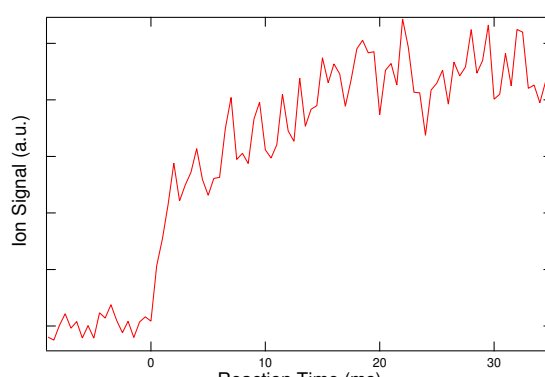


(c)

**Figure 3:** PI curves of propene[37] (blue line) superimposed onto the experimental photoionization plot of  $m/z = 42$  recorded at (a) 550 K and (b) 650 K. (c) Time trace of  $m/z = 42$  compared to the time trace of  $m/z = 58$  at 650 K.



(a)



(b)

**Figure 4:** (a) Experimental photoionization plot of  $m/z = 43$  fragment recorded at 550 K; (b) Experimental kinetic trace of  $m/z = 43$  from 0 (trigger time) to 30 ms at 550 K as well.

At  $m/z = 58$  a peak is recorded in all experiments, as shown in Figure 1. Figure 5 shows the experimental photoionization plots of  $m/z = 58$  product at different temperatures along with the PI curves taken from the literature with the aim of characterizing an overall isomeric composition. The experimental onset is  $9.67 \pm 0.05$  eV, which is in agreement with the literature AIE measurement of  $9.694 \pm 0.006$  eV for acetone.[39] In addition, acetone PI spectrum by Cool et al.[37] perfectly matches the very first part of the experimental PI curve, which confirms this assignment. A second feature is found at 9.96 eV, where the experimental signal raises deviating from acetone PI curve. This can be ascribed to the pres-

ence of propanal. Its AIE literature determination is  $9.96 \pm 0.01$  eV from Linstrom[40], consistent with the experimental observed spectral shoulder. The summation of the PI literature curves of acetone[37] and propanal[41] is in accordance with the experimental plot of  $m/z = 58$  at all three temperatures. The relative intensities of the two isomers vary at different temperatures, therefore, revealing an effect of the temperature on the observed product yields.

$m/z = 61$  is detected at room temperature, while it almost disappears at 550 and 650 K. Since this is an odd mass, there are only two feasible options to be considered for establishing its identity: it can be either attributed to a radical species, which ionizes to give the  $m/z = 61$  cation, or it can be ascribed to a cationic fragment coming from dissociative photoionization of a larger species. Since the kinetic trace of this mass (see Figure 6b) does not show a usual radical behaviour, it can be solely assigned to a dissociative photoionization fragment.

Furthermore,  $m/z = 61$  is not very common in mass spectrometry and a limited number of chemical compounds can be used to explain its formation. By taking into account the chemical structure of DIPE, isopropyl acetate (hereafter: IPAC) has been proposed. Benoit et al.[42] found  $m/z = 61$  to derive from fragmentation of isopropyl acetate ( $m/z = 102$ ) molecular ion, whose intensity is extremely low due to its cation ground state instability. They also reported the appearance energy value of  $9.96 \pm 0.05$  eV, consistent with the experimental value of this work, which is  $10.03 \pm 0.05$  eV. An absolute photoionization spectrum has been recorded as well confirming the presence of IPAC, as illustrated in Figure 7.

The occurrence of IPAC has been found out in previous studies, where it is clearly shown as being the major product of DIPE photooxidation.[14, 15, 43] Nevertheless, experimental conditions were substantially different owing to high concentration of NO and HO<sub>2</sub> radicals. There is solely one way to yield IPAC starting from DIPE in the absence of either NO and HO<sub>2</sub>, which involves self-reaction of alkylperoxy radicals ( $ROO^*$ ) to form alkylalkoxy radicals ( $RO^*$ ), followed by an  $\alpha$ - $\beta$ -cleavage (C-C bond fission) resulting into IPAC together with a methyl group release. Several studies[44–50] supported a concerted Russell

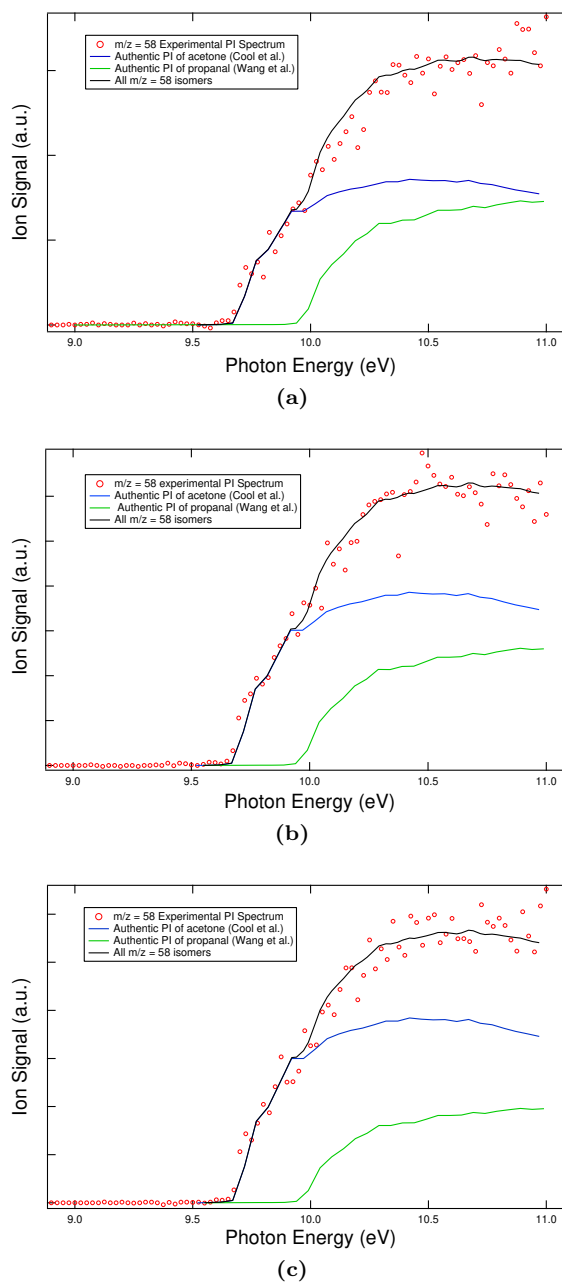


**Figure 5:** PI curves of acetone[37] (blue line) and propanal[41] (green line) superimposed onto the experimental photoionization plot of  $m/z = 58$  product recorded at (a) 298 K, (b) 550 K, and (c) 650 K.

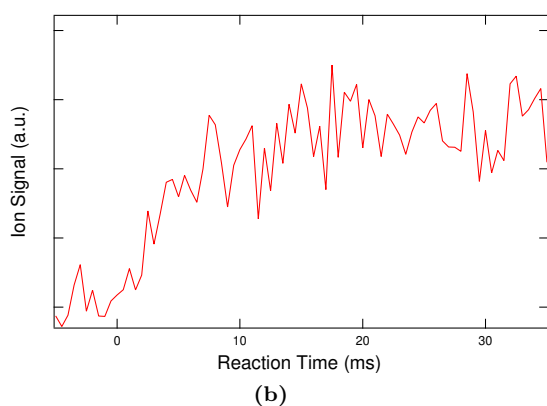
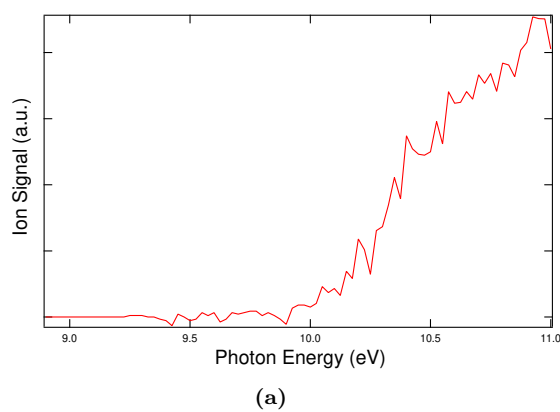


**Figure 6:** (a) Experimental photoionization plot of  $m/z = 61$  fragment recorded at room temperature; (b) Experimental kinetic trace of  $m/z = 61$  from 0 (trigger time) to 30 ms at room temperature as well.

arrangement[51, 52] passing through a tetraoxide intermediate for secondary  $ROO^*$  or a cage-mechanism for tertiary  $ROO^*$ , where few  $RO^*$  escape the cage along with  $O_2$  and, then, they undergo C-C bond fission.[53, 54]  $m/z = 61$  kinetic trace, which is equal to the parent ion kinetic trace, suggests a fast formation consistent with a Russell mechanism rather than a cage mechanism. However, since the characterization of secondary products lies beyond the purpose of this study, we cannot neither confirm nor dismiss any mechanisms leading to the formation of IPAC.

A peak at  $m/z = 59$  is recorded only at room temperature. The intensity does not match the real iso-

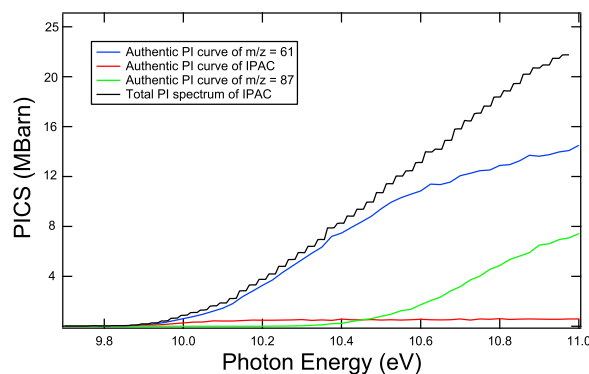


**Figure 7:** Authentic experimental photoionization spectrum of isopropyl acetate.

topic abundance of  $m/z = 58$ , which is expected to be 3.3 % ( $^{13}C$ ). Plus, the kinetic trace of  $m/z = 59$  appears totally different from mass 58 (see Figure 8), implying that this signal corresponds to another species.

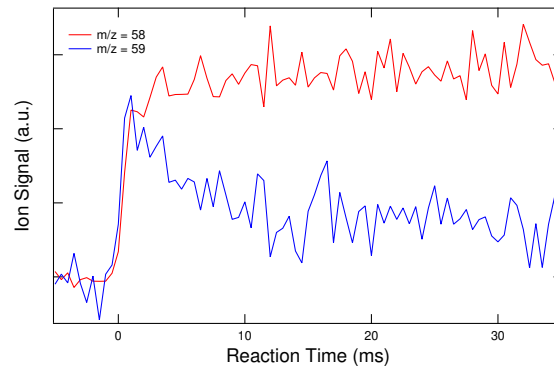


**Figure 8:** Experimental kinetic traces of  $m/z = 58$  (red line) and  $m/z = 59$  (blue line) from 0 to 30 ms at room temperature.

Calculations have been performed to establish if it comes from ionization of a radical or from fragmentation of a dissociatively photoionizing compound. It was thought to derive from C-O bond fission of alkylalkoxy radicals ( $RO^*$ ) yielding a 1-methyl ethoxy radical along with acetone. The corresponding Gibbs activation energy for this path is calculated to be  $87 \text{ kJ mol}^{-1}$  at room temperature, while the

Gibbs reaction energy is  $-19 \text{ kJ mol}^{-1}$ . In addition, William and Hamill[33] found  $m/z = 59$  ascribed to 1-methyl ethoxy radical generated by passing DIPE gas through a platinum wire "cracker". The relative AIE was  $9.20 \pm 0.05 \text{ eV}$ , although we measure an onset at  $9.60 \pm 0.05 \text{ eV}$ . Despite the computational efforts, no satisfactory results have been achieved in this direction, thus we ascribe this species to a fragment of  $RO^*$  photodissociation resulting into  $m/z = 59$  cation along with  $m/z = 58$ . Taking into account the instability of this radical, we can justify the  $m/z = 59$  kinetic trace as coming from  $RO^*$  fast formation and depletion.

At room temperature a low intensity peak appears at  $m/z = 100$ , gradually disappearing as the temperature increases. Unfortunately, there are not available PI spectra from literature to characterize  $m/z = 100$ . According to postulated mechanisms (see below), we performed PI spectra simulations of feasible compounds having  $m/z = 100$ , i.e., 2,5-dimethyltetrahydrofuran (hereafter: 25DMTHF) and isopropyl isopropenyl ether (hereafter: IIE). The 25DMTHF simulated PI spectrum matches the onset of the experimental  $m/z = 100$  spectrum, whereas the IIE simulated PI spectrum does not match any feature of the experimental data (see Figure 9).

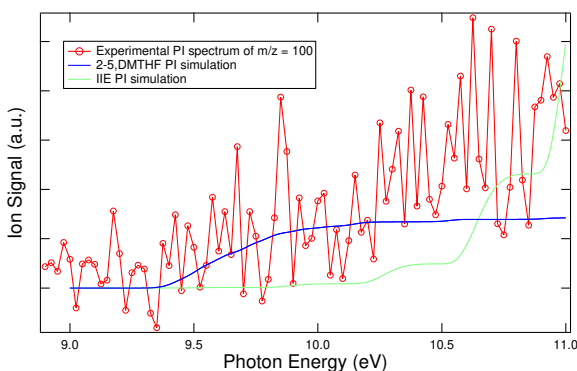
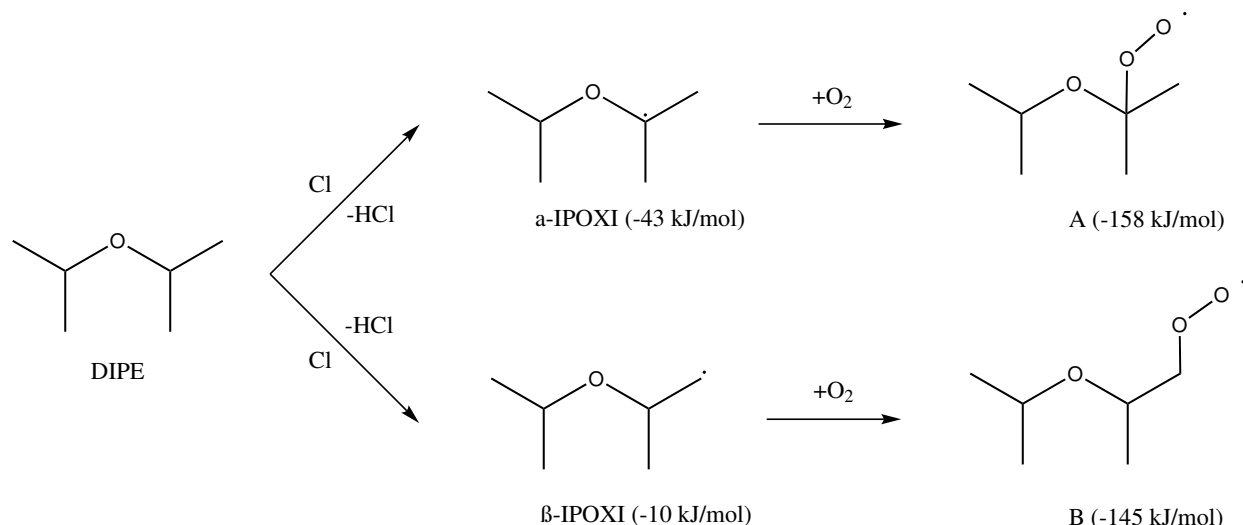


**Figure 9:** PI spectra simulations of 25DMTHF (blue line) and IIE (green line) superimposed onto the experimental photoionization plot of  $m/z = 100$ .

**Postulated Mechanisms.** Two distinct possible sites from DIPE are expected to undergo a hydrogen abstraction by atomic chlorine radicals to form alkyl

radicals ( $RO^*$ ) as illustrated in Scheme 1. The first sites are the  $\alpha$ -carbons on both sides of the molecule, which give isopropoxy-2-isopropyl radical (hereafter:  $\alpha$ -IPOXI) along with HCl. The CBS-QB3-calculated enthalpy change of this process is  $-43 \text{ kJ mol}^{-1}$ . The second equivalent sites where chlorine can abstract a hydrogen are the four  $\beta$ -carbons, from which isopropoxy-1-isopropyl radical (hereafter:  $\beta$ -IPOXI) along with HCl is generated with a calculated reaction enthalpy of  $-10 \text{ kJ mol}^{-1}$ .  $\alpha$ -IPOXI production results to be the most exothermic because  $\alpha$ -carbon is a secondary carbon stabilized by inductive effect from methyl groups. Indeed, Wallington and co-workers[43] found that secondary carbons are more reactive than primary carbons (80 % secondary vs. 20 % primary) at room temperature, with a reactivity increase of primary carbon sites expected to occur at higher temperatures. This is in agreement with previous studies[55, 56], where the vicinity of the oxygen has shown to weaken the C-H bond making the abstraction at this site more favorable than at the primary-carbon site. Further, Scheme 1 shows  $O_2$  addition to the radical site yielding alkoxyalkylperoxy radicals ( $RO^*OO^*$ ):  $\alpha$ -ROO (A) and  $\beta$ -ROO (B). These species can undergo intramolecular hydrogen abstraction with the consequent isomerization to hydroperoxyalkoxyalkyl radicals (hereafter: QOOH). Then, labile QOOH radicals can undergo unimolecular dissociation to form several products, which are not all experimentally-observed in this study, by means of  $\alpha$ - $\beta$  cleavages and cyclization processes as detailed in the following section.

**$\alpha$ -IPOXI Reaction Pathway.**  $\alpha$ -IPOXI radical reacts with  $O_2$  to give  $\alpha$ -peroxy radical ( $\alpha$ -ROO), with a calculated reaction enthalpy equal to  $-158 \text{ kJ mol}^{-1}$ .  $\alpha$ -ROO, then, undergoes a unimolecular process, which consists of a hydrogen shift from the  $\alpha$ - or  $\beta$ -carbons of the isopropyl side to the oxygen of the other side to yield the resulting  $\alpha$ -QOOH (A1) and  $\beta$ -QOOH (A2) as shown in Scheme 2A. H-shift isomerization, as described above, has been found to be important in the oxidation process under low-NO and low- $HO_2$  conditions[15], which are fairly replicated in this study because of the total absence of NO. The corresponding activation enthalpies for these reactions are  $68$  and  $95 \text{ kJ mol}^{-1}$ , whereas the

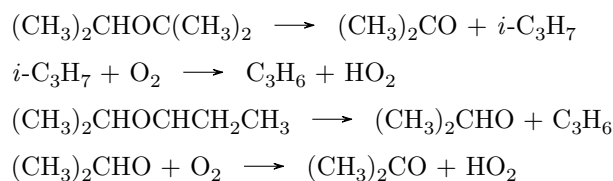


**Scheme 1:** Schematics of reaction pathways referring to Cl-initiated H-abstraction and subsequent  $O_2$  addition to form alkoxyalkylperoxy radicals ( $ROROO^*$ ). The CBS-QB3 calculated enthalpy of H-abstraction reactions are reported in parentheses

reaction enthalpies are 48 and 92  $kJ mol^{-1}$ , which are endothermic using A as the zero energy level, as well as far below the thermochemical threshold (red line in Schemes 2A and 2B) allocated to the  $\alpha$ -IPOXI +  $O_2$  energy level. Everything above the thermochemical threshold is considered to be thermodynamically unfavourable.  $\alpha$ -QOOH (A1) may decompose through a C-O bond fission leading to the formation of two molecules of acetone along with OH. The driving path from A1 to acetone is calculated to be exothermic with an energy release of -144  $kJ mol^{-1}$ .  $\beta$ -QOOH (A2) may decompose through a C-C bond fission leading to acetone and propene along with  $HO_2$  radical, which is calculated to stand above the thermochemical threshold, thus not feasible with respect to energetics. However, A2 can undergo a cyclization path, where the terminal methyl radical joins to the peroxy oxygen on the other side, yielding the five-membered ring compound 2,2,4-trimethyl-1,3-dioxolane ( $m/z = 116$ ,  $C_6H_{12}O_2$ ) together with a hydroxyl radical. The activation energy and the released reaction energy for this step are calculated to be 41  $kJ mol^{-1}$  and -192  $kJ mol^{-1}$ , respectively. Because of the high

activation barrier relative to A, this substituted dioxolane is not observed in our experiment. A fourth route to decomposition for  $\alpha$ -ROO radical species is the hydrogen abstraction on a  $CH_3$ -group of the same isopropyl side to obtain isopropyl isopropenyl ether and  $HO_2$ , which was shown to be energetically favourable with an activation enthalpy of 122  $kJ mol^{-1}$ . It is also predicted to arise via a concerted mechanism without involving any QOOHs isomer. A signal at  $m/z = 100$  is detected in the experiments at room temperature. Several studies[57–59] found unsaturated products formation by direct  $HO_2$  elimination from alkyl radicals reactions with  $O_2$ . Kaiser et al.[59], by investigating reactions of ethyl radicals with  $O_2$ ,  $Cl_2$ , and Cl, considered two different mechanisms yielding ethene: the first one deriving from ethyl radicals with  $O_2$  reactions, most probable at low pressure, and low Cl concentrations; whereas the second one coming from secondary reactions of long-lifetime Cl atoms with ethyl radicals, most probable at higher  $Cl_2$  concentrations and higher pressure. Unfortunately, the IIE PI spectrum simulation simulation did not allow us to reproduce the  $m/z = 100$  experimental plot, which is conversely in

agreement with 2,5-DMTHF PI spectrum simulation (see Figure 9). Since it was not possible to find a thermodynamically-favourable pathway yielding 2,5-DMTHF, this mass is considered a product from secondary reactions. As the temperature increases,  $m/z = 100$  progressively disappears and the  $m/z = 42$  signal, assigned to propene, comes up. Propene formation passes through chain-terminating reactions of isopropyl radicals with oxygen also yielding  $\text{HO}_2$ [60] and by  $\beta$ -IPOXI radicals decomposition. Isopropyl radicals come from the decomposition of  $\alpha$ -IPOXI radicals, which is increasingly expected to occur as the temperature grows, since decompositions are endothermic reactions. Below the above-mentioned reactions are illustrated:



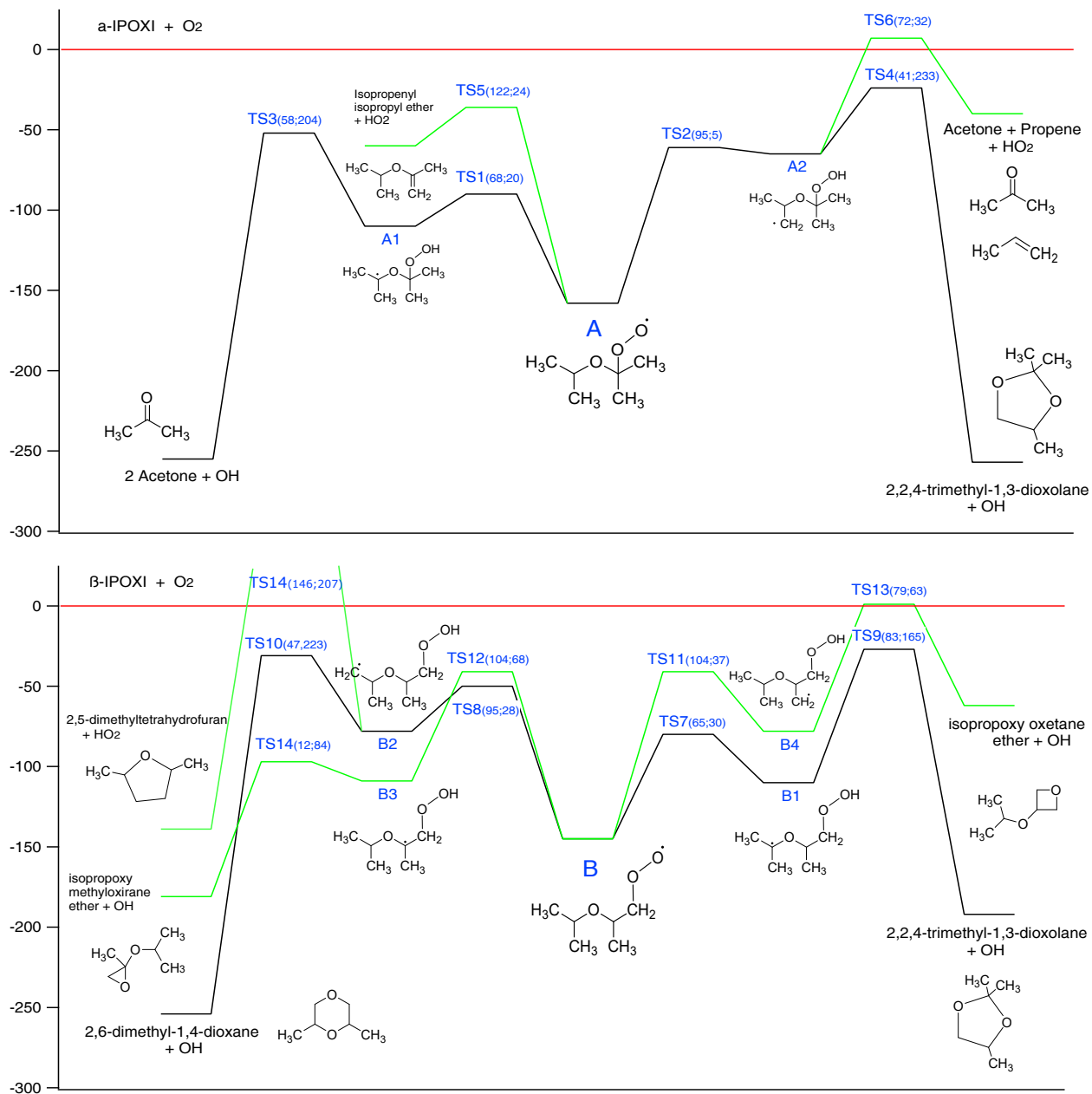
**$\beta$ -IPOXI Reaction Pathway.**  $\beta$ -IPOXI radical reacts with  $\text{O}_2$  to yield  $\beta$ -peroxy radical ( $\beta$ -ROO), with a calculated reaction enthalpy of  $-145 \text{ kJ mol}^{-1}$ .  $\beta$ -ROO, further, is expected to undergo similar unimolecular processes as  $\alpha$ -ROO, consisting of an intramolecular H-abstraction to yield several QOOH species as illustrated in Scheme 2B. When the hydrogen is removed from an  $\alpha$ -carbon of the other side, an  $\alpha$ -QOOH- $\beta$  (B1) is produced. This species can undergo the same cyclization as  $\beta$ -QOOH (A2) yielding the heterocyclic acetal, 2,2,4-trimethyl-1,3-dioxolane. If hydrogen on the  $\beta$ -carbon on the other side is extracted,  $\beta$ -QOOH- $\beta$  (B2) is generated. Even here, the attack of the methyl radical on the peroxydic oxygen gives a six-membered cyclic ether 2,6-dimethyl-1,4-dioxane ( $m/z = 116$ ,  $\text{C}_6\text{H}_{12}\text{O}_2$ ). Energy released is equivalent to  $-176 \text{ kJ mol}^{-1}$  with an activation energy of  $47 \text{ kJ mol}^{-1}$  with respect to B2. These cyclic species are not observed in our experiments most likely due to their high activation barriers relative to B. In the event that hydrogen is removed from the  $\alpha$ -carbon on the same side, a  $\beta$ -QOOH- $\alpha$

(B3) is formed. Here, the carbon binds to the peroxydic oxygen giving an oxyrane: isopropoxy methyloxirane ( $m/z = 116$ ). Reaction energy is estimated to be  $-72 \text{ kJ mol}^{-1}$  with respect to B3, with an activation energy of  $12 \text{ kJ mol}^{-1}$ . No corresponding observed signal for this species is due to its unbound cation dissociating into the isopropyl cation ( $m/z = 43$ ) and neutral methylene acetate ( $m/z = 73$ ). By using Equation 2, therefore, without considering a reverse barrier for dissociation (thermochemical limit), the calculated AE for  $m/z = 43$  is  $9.85 \text{ eV}$ , which is in perfect agreement with the measured AE for  $m/z = 43$  of  $9.85 \pm 0.05 \text{ eV}$ . We want to point out that this assignment is only tentative since we cannot discard other species that may dissociate photoionize yielding  $m/z = 43$ . Finally, in the case of hydrogen removal from the  $\beta$ -carbon on the same side, a  $\alpha$ -QOOH- $\alpha$  (B4) is created. The cyclization path leads to isopropoxy oxetane ( $m/z = 116$ ), which because of extremely low Franck-Condon factors due to the opening of the ring in the cation and high activation barrier cannot be observed. The reaction energy is  $-62 \text{ kJ mol}^{-1}$ , whereas the activation energy is  $78 \text{ kJ mol}^{-1}$ , with respect to B4. The transition state for this step stands marginally above the thermochemical threshold.  $\beta$ -IPOXI direct decomposition pathway is considered to be another source of propene at higher temperature experiments, since temperature enhances the reactivity of  $\beta$ -carbons promoting  $\beta$ -IPOXI radicals formation and subsequent decomposition.

**Branching Fractions.** Photoionization cross-sections, besides being important in products characterization, are also useful in quantitative analysis. Concentrations of primary products relative to the reactant, also known as branching fractions, are obtained taking the ratio of the observed ion intensity (see Equation 3) of a product (p) to the ion intensity of the reactant (r). The following equation is used:

$$\frac{C_p}{C_r} = \frac{\frac{S_p}{\sigma_p \delta_p}}{\frac{S_r}{\sigma_r \delta_r}} = \frac{S_p \sigma_r \delta_r}{S_r \sigma_p \delta_p} = \frac{S_p \sigma_r}{S_r \sigma_p} \left( \frac{m_r}{m_p} \right)^{0.67} \quad (5)$$

Since the photoionization cross-section and ion signal depend on the used photon energy, PI spectra



**Scheme 2: Decomposition pathways for  $\alpha$ -ROO (A) and  $\beta$ -ROO (B).** The red line indicates the reference energy level. The Y axis accounts for the relative energy expressed as  $\text{kJ mol}^{-1}$ . Numbers in parentheses correspond to energy barriers for the forward reaction (left value) and reverse reaction (right value) starting from the A or B species.

Chemical Name	m/z	298K	550K	650K
acetone	58	45 ±15%	83 ±29%	80 ±28%
isopropyl acetate	102	41 ±14%	-	-

**Table 1:** Branching fractions for reaction products at each experimental temperature calculated by integrating the ion intensities over a reaction time range from 20 to 50 milliseconds.

are compared at the same highest energy in these experiments (11 eV) where signal fluctuations are minimized. Absolute photoionization cross-section of acetone[37] was taken from literature. The overall uncertainty of each branching fraction is calculated using the propagation of the errors of all the quantities in Equation 5. The error of the ion signal is approximately 5 %, the error of  $\sigma_{DIPE}$ (11 eV) is 28 %, and the error of the mass discrimination factor is 3 % from reference.[35] Branching fractions relative to DIPE are listed in Table 1 with uncertainties.

The calculated fractions of acetone may be affected by possible secondary reactions, although based on the observed kinetic traces we cut off part of the signal related to high reaction time (signal integration is in the 0-30 ms range), thus cleaning up the spectra from secondary reactions as much as possible. We also want to point out the fact that one thermodynamically feasible product cannot be quantified because of its poor Franck-Condon factors (isopropoxy methyloxirane). Acetone is the only detected primary product. As the temperature increases, propene appears at both 550 K and 650 K experiments, suggesting a change in product-leading routes from 298 K to higher temperatures. Despite  $\beta$ -IPOXI radicals decomposition is considered to be a primary reaction to yield propene, it is also a product from secondary reactions involving isopropyl radicals, thus its branching fractions are not listed. Since it was not possible to find thermodynamically-favourable

pathways to form propanal and 2-5,DMTHF as primary products, we consider them as deriving from secondary chemistry, therefore, their branching fractions are not listed in Table 1 either. Even though IPAC derives from secondary reactions, it is a main product at room temperature. It is worthwhile to comment that this result suggests that at room temperature the oxidation reaction of DIPE proceeds via secondary reactions about 40-50 % of the time, most likely through the self-reactions of  $\alpha$ -ROO radicals. As the temperature increases this path becomes less relevant. The importance of the peroxy radicals self-reaction has been recently reported[51] and the mechanisms were investigated. No particular changes are noted when the temperature rises from 550 K up to 650 K. From m/z = 61 time trace, which shows the same time behavior of its parent ion IPAC and the measured branching fractions, we can obtain a rough estimate of the bimolecular rate constant ( $k_3$ ) at room temperature for the ROO self-reaction yielding IPAC by making some bold assumptions. The reaction is complete at 15 ms ( $t_3$ ) when approximately 45 % DIPE is consumed. Taking a concentration of  $\alpha$ -ROO radicals (A) of roughly  $8 \times 10^{11}$  molecule  $cm^{-3}$  (we are assuming that all Cl atoms, limiting reactant, yield  $\alpha$ -IPOXI radicals, which all react with  $O_2$  forming  $\alpha$ -ROO), the reaction proceeds with a  $k_3$  of  $1 \times 10^{-10}$  molecule $^{-1}$ cm $^3$ s $^{-1}$ . In addition, from m/z = 58 time trace and its measured branching fraction we can get a crude estimate of the unimolecular rate constant k to form acetone from A. The reaction is complete after 5 ms ( $t_1$ ) when 45 % of DIPE is depleted yielding a k of 160 s $^{-1}$ . If the rate determining step is the formation of  $\alpha$ -QOOH (A1), then  $k = k_1 \simeq 160$  s $^{-1}$ . Because of the measured branching fractions of the species coming directly from the ROO radical, i.e., acetone and IPAC, we can also derive  $k_1$  from the  $k_3$ , that is:

$$\frac{k_1}{2k_3[A]_0} = \frac{[Acetone]}{[IPAC]} = 1 \quad (6)$$

$$k_1 = 2 \frac{1}{t_3} \left( \frac{1}{0.45[A]_0} - \frac{1}{[A]_0} \right) \simeq 160s^{-1} \quad (7)$$

where 2 is due to the fact that 2A are needed to generate IPAC. This value is consistent with the one

obtained from the acetone time trace.

## 6 Conclusions

We studied the Cl-initiated oxidation reaction of DIPE at 298, 550, and 650 K, under low pressure conditions. Acetone has been detected as the main primary product. Branching fractions showed differences between the experiment at room temperature and higher temperatures. Indeed, the presence of isopropyl acetate in the experiment at room temperature suggests that a bimolecular channel is important despite the low pressure conditions. The isomerization of peroxy radicals leading to QOOHs followed by decomposition, i.e., unimolecular channel, is considered to be the source of acetone at room temperature. Since cyclic ethers are not observed at higher temperature, it seems that the cyclization pathway do not occur or are significantly reduced, due to the thermal decomposition of  $\alpha$ -IPOXI and  $\beta$ -IPOXI radicals, by C-O bond fission. These pathways are the major sources of acetone at higher temperatures. This finding results in agreement with a previous study[61], where thermal decomposition of radicals deriving from ethers has been found to be much faster than reaction with O<sub>2</sub> at 753 K. Propene time trace shows a slower formation typical of secondary chemistry processes. Most likely, propene formation passes through chain-terminating reactions of isopropyl radicals with O<sub>2</sub> also yielding HO<sub>2</sub> and by  $\beta$ -IPOXI radicals decomposition. Finally, because we did not find any thermodynamically-favorable pathways to explain propanal formation as primary product, we consider it as deriving from secondary chemistry.

## 7 Acknowledgment

This work is supported by the American Chemical Society Petroleum Research Fund Grant 56067-UR6. The authors express their gratitude to Drs. Taatjes and Osborn from Sandia National Laboratories for the utilization of SPIMS experimental apparatus. The Advanced Light Source is supported by the Di-

rector, Office of Science, Office of Basic Energy Sciences, of the U.S. Department of Energy under Contract No. DE-AC02-05CH11231. The authors also acknowledge Prof. Fabio Ramondo from the University of L'Aquila (Italy) and Dr. Leonid Sheps from the Combustion Research Facility of Sandia National Laboratories, who supported the authors on their work.

## 8 Keywords

Branching Fractions, Combustion, Diisopropyl Ether Oxidation, Multiplexed Synchrotron Photoionization Mass Spectrometry, Photoionization Cross-section, Primary Reactions, Secondary Reactions

## 9 TOC

Multiplexed synchrotron photoionization mass spectrometry has been employed to study the Cl-initiated oxidation of diisopropyl ether at 298, 550, and 650 K. Acetone, propanal, propene, and isopropyl acetate have been identified as major reaction products. Acetone is the main primary product at all temperatures. At 298 K almost 50% of the reaction proceeds via the self-reaction of the initial peroxy radical to yield isopropyl acetate.

## References

- [1] Gopinath Dhamodaran, Ganapathy Sundaram Esakkimuthu, and Yashwanth Kutti Pochareddy. *Fuel*, 173:37–44, 2016.
- [2] Ronald G. Harvey. *Polycyclic Aromatic Hydrocarbons*, 2011.
- [3] G. Grimmer. *Environmental Carcinogenics*, 2017.
- [4] B. J. Finlayson-Pitts. *Science*, 276(5315):1045–1051, 1997.
- [5] Clean Fuels Development Coalition. *Oxygenates Fact Book*, www.cleanfuelsdc.org, 2014.

- [6] J Yanowitz, E Christensen, and R L McCormick. Office of Scientific and Technical Information (OSTI), 2011.
- [7] V. D. Stytsenko, A. A. Lavarinenko, L. E. Nadra, and V. A. Vinokurov. *Chem. Technol. Fuels Oils*, 44(5):364–369, 2008.
- [8] Pamela M. Franklin, Catherine P. Koshland, Donald Lucas, and Robert F. Sawyer. *Environ. Sci. Technol.*, 34(18):3857–3863, 2000.
- [9] Environmental Protection Agency: State Actions Banning MTBE. 2007.
- [10] J. Sutherland and C. Adams. *Environ. Eng. Sci.*, 24(8):998–1005, 2007.
- [11] Matthew Winfough, Rong Yao, Martin Ng, Katherine Catani, and Giovanni Meloni. *J. Phys. Chem. A*, 121(7):1460–1469, 2017.
- [12] Tom Shih, Yue Rong, Thomas Harmon, and Mel Suffet. *Environ. Sci. Technol.*, 38(1):42–48, 2004.
- [13] Frank P. Heese, Mark E. Dry, and Klaus P. Möller. *Catal. Today*, 49(1-3):327–335, 1999.
- [14] E.M. Collins, H.W. Sidebottom, J.C. Wenger, S. Le Calvé, A. Mellouki, G. LeBras, E. Vilenave, and K. Wirtz. *J. Photochem. Photobiol., A*, 176(1-3):86–97, 2005.
- [15] Sainan Wang and Liming Wang. *Phys. Chem. Chem. Phys.*, 18(11):7707–7714, 2016.
- [16] David L. Osborn, Peng Zou, Howard Johnsen, Carl C. Hayden, Craig A. Taatjes, Vadim D. Knyazev, Simon W. North, Darcy S. Peterka, Musahid Ahmed, and Stephen R. Leone. *Rev. Sci. Instrum.*, 79(10):104103, 2008.
- [17] Craig A. Taatjes, Nils Hansen, David L. Osborn, Katharina Kohse-Höinghaus, Terrill A. Cool, and Phillip R. Westmoreland. *Phys. Chem. Chem. Phys.*, 10(1):20–34, 2008.
- [18] Amelia W. Ray, Craig A. Taatjes, Oliver Welz, David L. Osborn, and Giovanni Meloni. *J. Phys. Chem. A*, 116(25):6720–6730, 2012.
- [19] Martin Y. Ng, Brittany M. Bryan, Jordan Nelson, and Giovanni Meloni. *J. Phys. Chem. A*, 119(32):8667–8682, 2015.
- [20] IUPAC, Subcommittee on Gas Kinetic Data Evaluation - <http://iupac.pole-ether.fr>.
- [21] D. Maric, J.P. Burrows, R. Meller, and G.K. Moortgat. *J. Photochem. Photobiol., A*, 70(3):205–214, 1993.
- [22] Yasmin Fathi, Chelsea Price, and Giovanni Meloni. *J. Phys. Chem. A*, 121(15):2936–2950, 2017.
- [23] William A. Chupka and Joseph Berkowitz. *J. Chem. Phys.*, 47(8):2921–2933, 1967.
- [24] M. J. Frisch, G. W. Trucks, H. B. Schlegel, G. E. Scuseria, M. A. Robb, J. R. Cheeseman, G. Scalmani, V. Barone, B. Mennucci, G. A. Petersson et al. Gaussian 09, 2009.
- [25] J. A. Montgomery, M. J. Frisch, J. W. Ochterski, and G. A. Petersson. *J. Chem. Phys.*, 110(6):2822–2827, 1999.
- [26] J. A. Montgomery, M. J. Frisch, J. W. Ochterski, and G. A. Petersson. *J. Chem. Phys.*, 112(15):6532–6542, 2000.
- [27] Wolfgang Quapp. *Theor. Chem. Acc.*, 121(5-6):227–237, 2008.
- [28] D. L. Baulch, C. T. Bowman, C. J. Cobos, R. A. Cox, Th. Just, J. A. Kerr, M. J. Pilling, D. Stocker, J. Troe, W. Tsang, R. W. Walker, and J. Warnatz. *J. Phys. Chem. Ref. Data*, 34(3):757–1397, 2005.
- [29] Fabrizio Santoro, Roberto Improta, Alessandro Lami, Julien Bloino, and Vincenzo Barone. *J. Chem. Phys.*, 126(8):084509, 2007.
- [30] Terrill A. Cool, Andrew McIlroy, Fei Qi, Phillip R. Westmoreland, Lionel Poisson, Darcy S. Peterka, and Musahid Ahmed. *Rev. Sci. Instrum.*, 76(9):094102, 2005.
- [31] Matthew A. Oehlschlaeger, David F. Davidson, and Ronald K. Hanson. *J. Phys. Chem. A*, 110(32):9867–9873, 2006.

- [32] Mingfeng Xie, Zhongyue Zhou, Zhandong Wang, Dongna Chen, and Fei Qi. *Int. J. Mass Spectrom.*, 293(1-3):28–33, 2010.
- [33] James M. Williams and William H. Hamill. *J. Chem. Phys.*, 49(10):4467–4477, 1968.
- [34] K. Watanabe, Toshio Nakayama, and Joseph Mottl. *J. Quant. Spectrosc. Radiat. Transfer*, 2(4):369–382, 1962.
- [35] Oliver Welz, Judit Zádor, John D. Savee, Martin Y. Ng, Giovanni Meloni, Ravi X. Fernandes, Leonid Sheps, Blake A. Simmons, Taek Soon Lee, David L. Osborn, and Craig A. Taatjes. *Phys. Chem. Chem. Phys.*, 14(9):3112, 2012.
- [36] John C. Traeger. *Int. J. Mass Spectrom. Ion Processes*, 58:259–271, 1984.
- [37] Terrill A. Cool, Juan Wang, Koichi Nakajima, Craig A. Taatjes, and Andrew McIlroy. *Int. J. Mass Spectrom.*, 247(1-3):18–27, 2005.
- [38] John Dyke, Andrew Ellis, Neville Jonathan, and Alan Morris. *J. Chem. Soc., Faraday Trans. 2*, 81(10):1573–1586, 1985.
- [39] Wayne M. Trott, Normand C. Blais, and Edward A. Walters. *J. Chem. Phys.*, 69(7):3150–3158, 1978.
- [40] Linstrom. <http://webbook.nist.gov>, 2005.
- [41] Juan Wang, Bin Yang, Terrill A. Cool, Nils Hansen, and Tina Kasper. *Int. J. Mass Spectrom.*, 269(3):210–220, 2008.
- [42] F. M. Benoit, A. G. Harrison, and F. P. Lossing. *Org. Mass Spectrom.*, 12(2):78–82, 1977.
- [43] Timothy J. Wallington, Jean M. Andino, Alan R. Potts, Sara J. Rudy, Walter O. Siegl, Zhengyu Zhang, Michael J. Kurylo, and Robert E. Huie. *Environ. Sci. Technol.*, 27(1):98–104, 1993.
- [44] Richard R. Hiatt and Katherine C. Irwin. *J. Org. Chem.*, 33(4):1436–1441, 1968.
- [45] Richard R. Hiatt, Theodore Mill, Katherine C. Irwin, and Jane K. Castleman. *J. Org. Chem.*, 33(4):1421–1428, 1968.
- [46] Richard R. Hiatt, Theodore Mill, and Frank R. Mayo. *J. Org. Chem.*, 33(4):1416–1420, 1968.
- [47] R. Hiatt and Ludek Zigmund. *Can. J. Chem.*, 48(24):3967–3969, 1970.
- [48] J. A. Howard and K. U. Ingold. *Can. J. Chem.*, 46(16):2655–2660, 1968.
- [49] J. A. Howard and J. E. Bennett. *Can. J. Chem.*, 50(14):2374–2377, 1972.
- [50] K. Adamic, J. A. Howard, and K. U. Ingold. *Can. J. Chem.*, 47(20):3803–3808, 1969.
- [51] Audrey R. Smith, Simone Di Muzio, Fabio Ramondo, and Giovanni Meloni. *Phys. Chem. Chem. Phys.*, 21(20):10228–10237, 2019.
- [52] Glen A. Russell. *J. Am. Chem. Soc.*, 79(14):3871–3877, 1957.
- [53] D. Lindsay, J. A. Howard, E. C. Horswill, L. Iton, K. U. Ingold, T. Cobbley, and A. Ll. *Can. J. Chem.*, 51(6):870–880, 1973.
- [54] Richmond Lee, Ganna Gryn'ova, K. U. Ingold, and Michelle L. Coote. *Phys. Chem. Chem. Phys.*, 18(34):23673–23679, 2016.
- [55] Peter McLoughlin, Rosaleen Kane, and Imelda Shanahan. *Int. J. Chem. Kinet.*, 25(3):137–149, 1993.
- [56] Linda Nelson, Oliver Rattigan, Ruaidhri Neavyn, Howard Sidebottom, Jack Treacy, and Ole John Nielsen. *Int. J. Chem. Kinet.*, 22(11):1111–1126, 1990.
- [57] Craig A. Taatjes. *J. Phys. Chem. A*, 110(13):4299–4312, 2006.
- [58] Adam M. Scheer, Oliver Welz, Judit Zádor, David L. Osborn, and Craig A. Taatjes. *Phys. Chem. Chem. Phys.*, 16(26):13027–13040, 2014.

- [59] E. W. Kaiser, L. Rimai, and T. J. Wallington. *J. Phys. Chem.*, 93(10):4094–4098, 1989.
- [60] Edgar G. Estupiñán, Stephen J. Klippenstein, and Craig A. Taatjes. *J. Phys. Chem. B*, 109(17):8374–8387, 2005.
- [61] R. S. Tranter and R. W. Walker. *Phys. Chem. Chem. Phys.*, 3(21):4722–4732, 2001.